Structure-Activity-Relationship Exploration and Animal Validation of a Novel Assembly Modulator Small Molecule Chemical Series with Pan-Cancer Selective Cytotoxicity

Authors

Anuradha F. Lingappa[1], Suguna Mallesh[1], Maya Michon[1], Devaraju Shivarudraswamy[1], Jim Lin[1], Dharma Prasad[1], Debendranath Dey[1], Dennis Solas[1], Vishwanath R. Lingappa[1,2,3]

[1] Prosetta Biosciences, Inc. 670 5th St San Francisco, CA 94107

[2] University of California, San Francisco

[3] To whom correspondence should be addressed.

Abstract

We recently described a novel class of chemical compounds initially identified as modulators of host-catalyzed HIV capsid assembly, that have been advanced to display broad anti-tumor cytotoxicity. Here we explore in more detail the structure-activity-relationship (SAR) of the chemical series. PAV-0805, an advanced analog, was found to be nontoxic at 10mg/kg in mice and nontoxic to healthy human peripheral blood mononuclear cells (PBMCs). PAV-0805 has broad anti-cancer activity in the NCI-60 cancer cell line screen, exhibiting cytotoxicity to a diversity of brain, breast, colon, lung, ovarian prostate, renal, and skin and blood cancers. In the aggressive 4T1 mouse allograft breast cancer model, PAV-0805 reduced tumor growth and metastasis when treatment was initiated early (primary tumor volume of $50mm^3$) or late (primary tumor volume of $500mm^3$). In both cases, treatment with PAV-0805 inhibited both tumor growth and metastasis to a degree comparable to early treatment with paclitaxel. PAV-0805 targets Protein Disulfide Isomerase in a dynamic multi-protein complex comprised of gene products involved in the cancer hallmarks of resisting cell death and reprogramming energy metabolism.

Introduction

PAV-951, the parent of the advanced molecule PAV-0805 to be discussed here, is a novel small molecule first identified as a modulator of host catalyzed HIV capsid formation in a cell-free protein synthesis and assembly (CFPSA) system, and validated against infectious virus in mammalian cells[1].

Cell-free systems have played an important role in the history of biochemistry and molecular cell biology. Such a system was used in the 19th century to demonstrate that fermentation of sugar to alcohol is possible outside living cells, in the 1960's to decipher the genetic code, and in the 1970's to establish the signal hypothesis of subcellular protein localization[2–4]. We applied CFPSA in yet another way: to reproduce features of viral capsid formation. Upon determining that capsid assembly occurs via an energy-dependent, host-catalyzed pathway, rather than by spontaneous self-assembly, as classically

believed, we adapted the CFPSA system into phenotypic screens for identifying antiviral small molecules, by virtue of their modulation of capsid formation. Advanced compounds from these screens have been shown to disruption of critical protein-protein interactions at the host-viral interface[5–11].

Historically, the discovery of new drug targets has involved a combination of initial serendipity followed by detailed structural biology to identify the drug binding site. While this works well for advancement of small molecules that block enzyme active sites and receptor binding sites, it has been less satisfactory for identification of allosteric sites. In part this is because identifying allosteric sites is technically difficult. In part also it is because multi-protein complexes likely have a large number of allosteric sites and identifying the most pathophysiologically relevant ones is even more challenging.

Viruses, however, identified their targets through natural selection over deep evolutionary time. Thus, our approach uses viruses as “trufflehounds” to reveal the fruits of viral natural selection and then adapts it to antiviral drug discovery. A benefit of a CFPSA-based phenotypic screen is that it is in relative slow motion, compared to the blinding speed of protein-protein interactions in the crowded environment of a living cell[12]. Finally, the phenomenon of protein “moonlighting” where by one gene product plays multiple different biological roles, greatly complicates strategies based on use of recombinant protein or cloned gene expression, as it is not clear to what extent the structural basis for the observed diversity of function is revealed by those methods.

PAV-951, identified first by inhibition of HIV capsid formation through CFPSA and then validated against infectious HIV in cell culture, was counterscreened against cancer cell lines[1]. While unorthodox, our pursuit of anti-viral compounds for cancer therapeutics has a compelling logic. A vast body of literature connects viruses with cancer[13–15]. Oncogenic viral proteins facilitate viral propagation and predispose cells to tumorigenesis by various methods, including the disruption or modification of biochemical pathways which are critical for maintaining homeostasis and cell cycle control[15,16].

Human Papilloma Virus (HPV) is a well-studied example of an oncogenic virus[15,17]. HPV E7 viral proteins have no known intrinsic enzymatic activities, but they are observed to associate with and modify the functions of cellular protein complexes[15,17–21]. HPV E7 viral protein is itself oncogenic— expression of HPV E7 in a transgenic mouse is sufficient for cervical cancer development[22]. Likewise, in patients with both early and advanced stages of cervical cancer, elevated expression of HPV E7 positively correlates to a high HPV viral load[23]. Since viruses exploit underlying weak links in cellular homeostasis as a means of hijacking host protein machinery to facilitate capsid assembly, we hypothesized that our compounds which normalize protein-protein interactions at the host-viral interface might also restore diverse subcellular controls over programmed cell death that are disrupted in neoplastic cells[1].

PAV-951, the initial compound identified through our unique approach as both anti-viral *and* anti-cancer, displays a number of distinctive properties. First, its anti-cancer activity appears to be pan-cancer[1]. Anti-cancer activity was observed against 80 of 80 different tumor cell lines and in two mouse xenograft studies on lung and colon cancer[1], although the degree of efficacy varied substantially among the cancers tested. Second, its anti-cancer potency appears to be an order of magnitude improved when added to trypsinized cells at the time of plating, rather than to cells which have adhered to their growth matrix—conditions which model metastasis and suggest relevance to the epithelial-to-mesenchymal transition[1]. Third, the drug target appears to be a dynamic multi-protein complex[1].

From earlier work, including on structurally-unrelated assembly modulator compounds active in other therapeutic areas, we hypothesize that the multi-protein complex drug target of PAV-951 is an "assembly machine".[1,5,24,25] Assembly machines in healthy cells are hypothesized to contribute to maintenance of homeostasis[1,5,9,24,25]. Disease advances when assembly machine function, or the normal cellular response to it, is disabled, and has been correlated to a change in the protein composition of the multi-protein complex[1,5,24,25]. In the case of viral infection, the structurally altered multi-protein complex "aberrant assembly machine" is redirected to viral needs, including capsid assembly. Moreover, host

defenses are silenced[5–9,11,24]. In the case of cancer, the aberrant assembly machine is, directly or indirectly, not adequately responsive to uncontrolled proliferation or another hallmark of cancer[1,24].

Within the framework outlined above, both viruses and cancer take advantage of the patient's underlying assembly machinery and repurpose it for their own ends. In other therapeutic areas, we have observed that advanced chemical analogs of assembly modulator compounds are substantially selective for aberrant assembly machines[5,25,26]. This has been demonstrated empirically in biochemical experiments where advanced assembly modulators have lower affinity for their target in healthy cells, compared to diseased cells[5,26]. Correspondingly, these advanced analogs are strikingly non-toxic in animals. While the molecular basis for these observations remains to be determined, we speculate that they are a consequence of targeting allosteric sites in a selective manner that can both distinguish between assembly machines carrying out functions which maintain homeostasis and functions which deviate from homeostasis and drive disease.

Here, we extend this framework to cancer. We demonstrate superior safety while maintaining pan-cancer potency, for advanced cancer chemotype analogs. Biochemical methods are used to elucidate the functional target and develop a testable hypothesis on the mechanism of action of this novel anti-cancer drug.

Results

Structure-Activity-Relationship Exploration of Pan-Cancer Assembly Modulating Series

Chemical analogs of PAV-951 were assessed in the National Cancer Institute 60 cell line screen (NCI-60). Compounds were tested against up to 60 tumor cell lines (CCRF-CEM, HL-60(TB), K-562, MOLT-4, RPMI-8226, SR, A549/ATCC, EKVX, HOP-62, HOP-92, NCI-H226, NCI-H23, NCI-H322M, NCI-H460, NCI-H522, COLO 205, HCC-2998, HCT-116, HCT-15, HT29, KM12, SW-620, SF-268, SF-295, SF-539, SNB-19, SNB-75, U251, LOX IMVI, MALME-3M, M14, MDA-MB-435, SK-MEL-2, SK-

MEL-28, SK-MEL-5, UACC-257, UACC-62, IGROV1, OVCAR-3, OVCAR-4, OVCAR-5, OVCAR-8, NCI/ADR-RES, SK-OV-3, 786-0, A498, ACHN, CAKI-1, RXF 393, SN12C, TK-10, UO-31, PC-3, DU-145, MCF7, MDA-MB-231/ATCC, HS 578T, BT-549, T-47D, MDA-MB-468) at a single dose of 2.5uM. See **Figure 1** for NCI-60 data on PAV-951 and 14 of its chemical analogs.

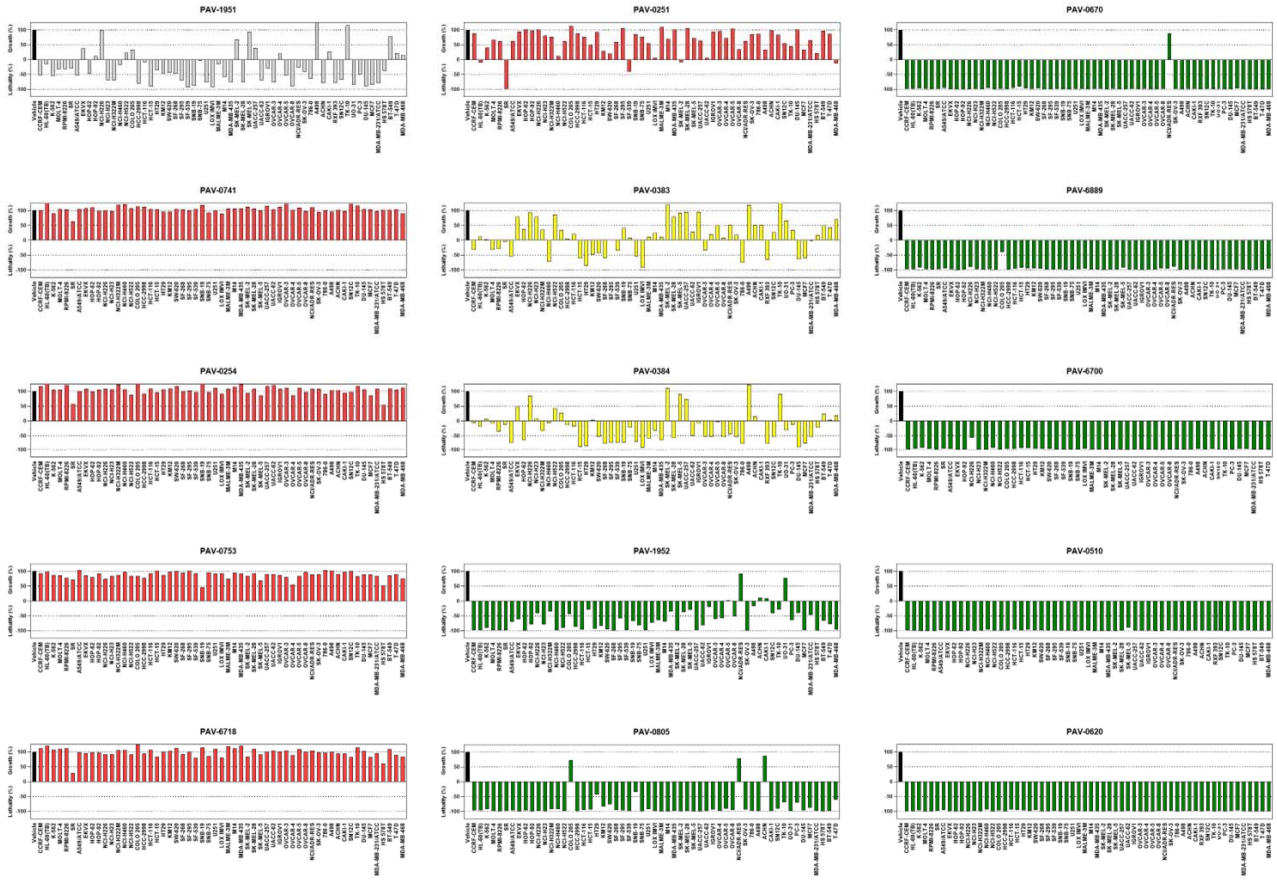

Figure 1. Anti-cancer assessment in the NCI-60 Screen. NCI-60 activity at a single dose of 2.5uM is shown for a set of chemical analogs based on PAV-951. Each bar represents a different tumor cell line. Cell viability of each cancer upon drug treatment is shown relative to the vehicle treated control and number of cells at time 0. Values between 0 and 100 represent percent growth inhibition. Values between 0 and -100 represent percent cellular lethality. Graphs are color coded

where red indicates loss, green indicates gain, and yellow indicates no substantial change in the anti-cancer activity of analogs compared to the parent compound.

Safety of active compounds was assessed in BALB/c mice. Increasing doses of compounds were administered to the mice by intraperitoneal (IP) injection. The highest dose which yielded no symptoms of toxicity 24 hours post-dose, was determined to be the MTD. Analogs were identified with 2-4x increases to safety relative to the parent compound, PAV-951. See **Figure 2A** for a table of single-dose mouse MTD.

Two compounds, PAV-0620 and PAV-0805, were assessed in mice through multi-day safety studies. The compound was administered at 10mg/kg twice daily to three male and three female BALB/c mice. All mice given PAV-0620 exhibited lethargy on the third day of dosing. Mice given PAV-0805 exhibited no clinical signs of toxicity after 15 days of twice daily dosing at 10mg/kg.

To define the therapeutic window of PAV-0805, we tested it against healthy PBMCs versus H9 lymphoma cells, in parallel under matched conditions. Cells were seeded at a density of 5,000 cells/well and treated with either DMSO or compound, at concentrations of 2.5uM, 5uM, 10uM, and 20uM. The cells were incubated at 37oC for 72 hours then cell viability was measured using an AlamarBlue™ assay. PAV-0805 did not significantly reduce cell viability in PBMCs, even at the 20uM dose (See **Figure 2B**). However, PAV-805 showed dose-dependent cytotoxicity to H9 lymphoma (See **Figure 2C**).

A.

Compound	Safe Dose (IP)
PAV-951	<5 mg/kg
PAV-0383	<5 mg/kg
PAV-0384	<5 mg/kg
PAV-0670	<5 mg/kg
PAV-0510	5 mg/kg
PAV-1952	5 mg/kg
PAV-6700	5 mg/kg
PAV-6889	5 mg/kg
PAV-0620	10 mg/kg
PAV-0805	10 mg/kg

B.

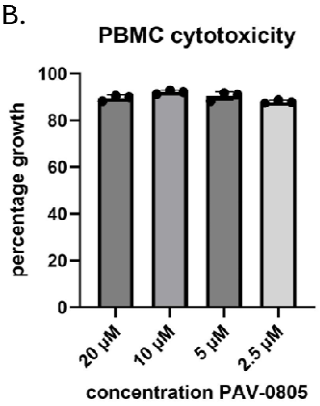

C.

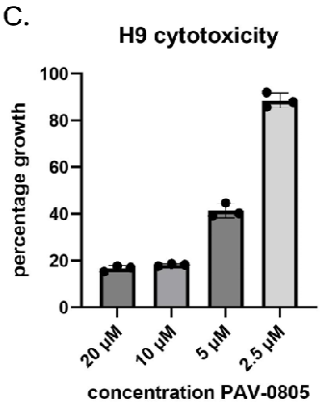

Figure 2. Safety of active chemical analogs. Figure 2A provides a table summarizing mouse safety for PAV-951 and 9 of its active analogs, by the metric of MTD by IP injection. Values are color coded where red indicates compounds that are not significantly safer than the parent compound, yellow indicates compounds that are at approximately 2x safer than the parent compound, and green indicates compounds that are approximately 4x safer than the parent compound. **Figures 2B** and **2C** show cell viability of normal PBMCs and cancerous lymphoma cells after 72 hours of treatment with 20uM, 10uM, 5uM, or 2.5uM PAV-0805. Graphs show cell viability in treated cells as a percentage of the cell viability measured in DMSO-vehicle treated cells.

Animal Validation of the Advanced Compound PAV-0805

The anti-cancer activity of PAV-0805 versus paclitaxel or DMSO was assessed in the 4T1 allograft mouse model. 4T1 is an aggressive triple negative breast cancer that spontaneously metastasizes in mice[27,28]. PAV-0805 was not assessed on the 4T1 cell line in advance of the study, but it was cytotoxic to MDA-MB-435 and MDA-MB-231, the cell lines in the NCI-60 screen which show characteristics of triple negative breast cancer[29]. After 4T1 cells are implanted in mice, a palpable tumor forms within a week and progresses to a tumor volume of >2,000 mm^3 within 30 days[27,28]. An advantage of using an

allograft model, in contrast to the xenograft studies which were used to assess PAV-951, is that the mice are immunocompetent and the interface between a test compound and the immune system is preserved.

A suspension of 0.1×10^6 4T1 cells were implanted into the mammary fat pad of BALB/c mice and tumor size was measured using a digital Vernier caliper. Tumor volume was calculated as the [Length (L) × Width (W) ^{2}] /2, where length (L) is the largest diameter of the tumor and width (W) is the smallest diameter. Tumor growth inhibition was calculated based on the following formula:

$$\% \text{ TGI} = \frac{\{(TV_{vehicle}\ \text{Final} - TV_{vehicle}\ \text{Initial}) - (TV_{treatment}\ \text{Final} - TV_{treatment}\ \text{Initial})\}}{(TV_{vehicle}\ \text{Final} - TV_{vehicle}\ \text{Initial})} \times 100$$

Animals were treated by IP injection daily with either vehicle (N=6), 2 mg/kg Paclitaxel (N=6), or 10mg/kg PAV-0805 (N=6), beginning when the tumor volume reached 50mm^3. An additional late treatment group (N=3) received vehicle until the tumor volume reached 500mm^3, followed by daily treatment with 10mg/kg PAV-0805 daily. Animals were sacrificed once the tumor in the vehicle-treated group reached a volume of 2000mm^3. Upon completion of the study, lung tissues were isolated and visually observed for metastatic cancer cell colonies.

In conditions where treatment began when the tumor was 50mm^3, Paclitaxel inhibited tumor growth by 42% and PAV-0805 inhibited tumor growth by 48% (See **Figure 3A**). When PAV-0805 was administered to a tumor that was at a volume of 500mm^3, it inhibited tumor growth by 38% (See **Figure 3A**). On average 82 lung nodules were found in vehicle-treated animals, 49 lung nodules were found in Paclitaxel-treated animals, 50 lung nodules were found in the PAV-0805 early-treatment group, and 53 lung nodules were found in the PAV-0805 late-treatment group (See **Figure 3B**). PAV-0805 treatment did not substantially impact body weight of the mice (See **Figure 3C**).

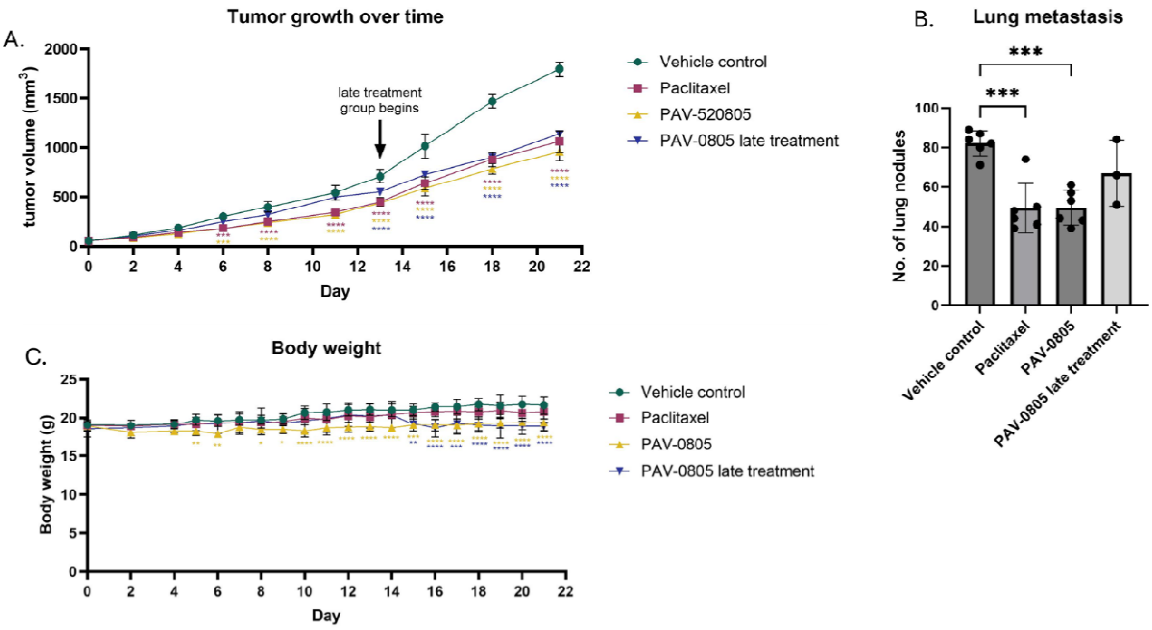

Figure 3. Efficacy of PAV-0805 in the 4T1 allograft model. 4T1 is an aggressive triple-negative mouse breast cancer cell line which spontaneously metastasizes in mice. In the allograft study, 4T1 tumors were implanted into immunocompetent BALB/c mice which were then treated with vehicle, 2 mg/kg Paclitaxel, or 10 mg/kg PAV-0805 given beginning when the tumor volume was $50mm^3$ or $500mm^3$. **Figure 3A** shows growth of the primary tumor over time, with statistical significance indicated based on 2-way anova and Dunnet's multiple comparisons test. **Figure 3B** shows quantitation of lung metastasis upon completion of the study with statistical significance indicated based on one-way anova and Dunnet's multiple comparisons test. **Figure 3C** shows body weight of mice during the study, with statistical significance indicated based on 2-way anova and Dunnet's multiple comparison test.

<u>Pan-Cancer Activity by Targeting the Hallmarks of Cancer</u>

PAV-951, the parent compound from the pan-cancer assembly modulator series, was determined to target a multi-protein complex by drug resin affinity chromatography (DRAC)[1]. PAV-0805 was coupled

to a resin from the same attachment point as PAV-951. DRAC with A549 cell extract was conducted in triplicate using the PAV- 0805 and PAV-951 resins in parallel and eluting with the cognate compound. PAV-951 was coupled to a resin, incubated with cancer cell extract, washed 100x to remove non-specifically bound proteins, and then eluted overnight with free drug.

The eluates from the PAV-0805 resin were analyzed by silver stain, western blot, and tandem mass spectrometry (MS-MS) analysis. Protein bands detected by silver stain showed that PAV-0805, like PAV-951, targets a set of proteins (see **Figure 4A**). The silver stains showed both an overlap between the sets of proteins targeted by PAV-951 and PAV-0805, and several differences between the proteins identified in the target of one compound but not the other (see **Figure 4A**). The MSMS analysis of PAV-0805 identified 181 proteins (See **Supplemental Figure 1** for the full list). Of these proteins 115, were not detected in the negative control resin eluate. Of those proteins, 29 were detected in all three triplicates (see **Supplemental Figure 1**).

Western blot of the eluates confirmed the MSMS findings including that PAV-951 and PAV-805 targeted similar amounts of ALDH1A1, meanwhile the target of PAV-951 contained more GSTP1, MDH, PDI, and PSMB5 than the target of PAV-0805, and the target of PAV-0805 contained more YWHAZ than

the target of PAV-951 (see **Figures 4B** and **4C**).

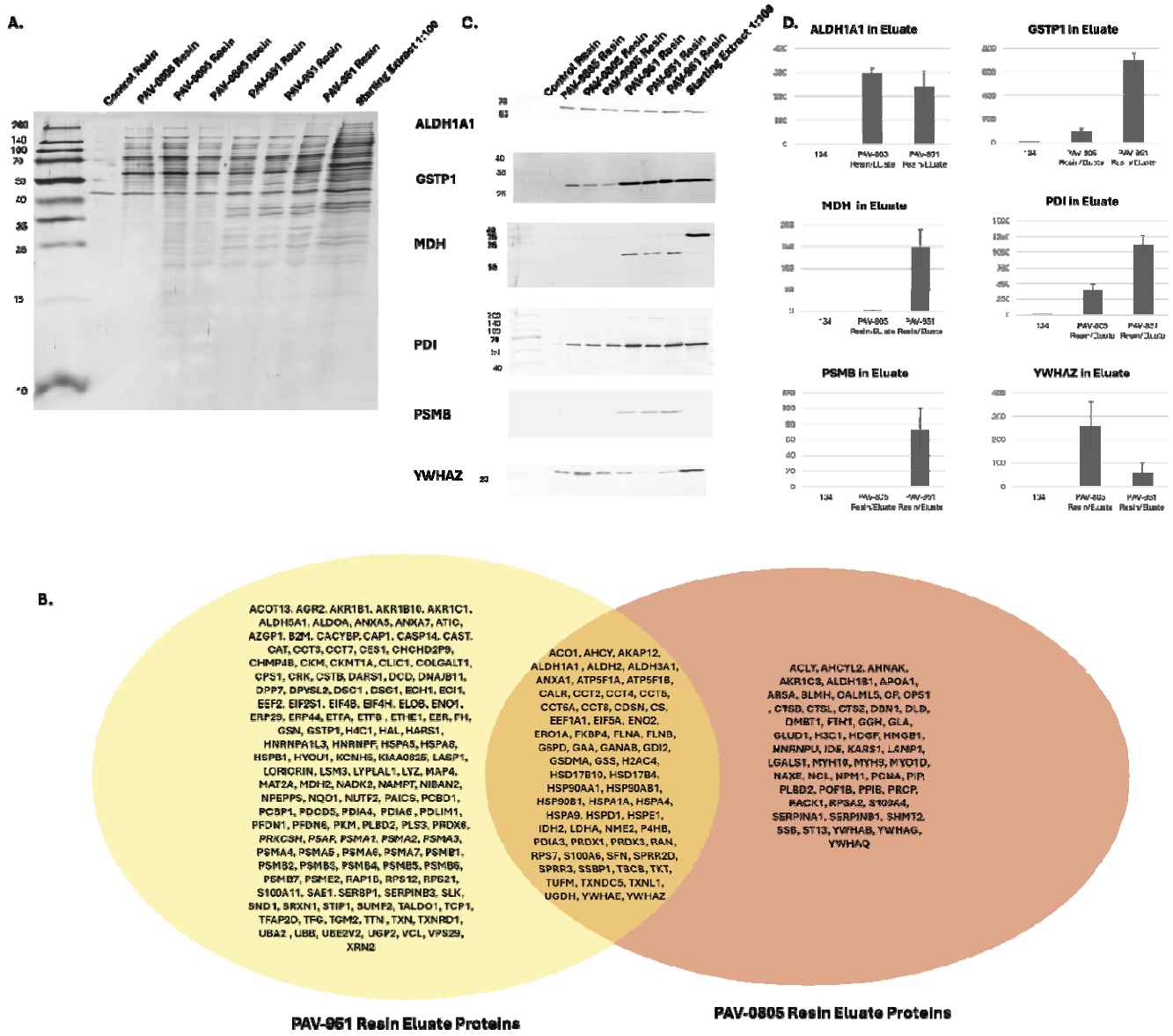

Figure 4. Comparison of PAV-951 and PAV-0805 Targets by DRAC. 30ul of 5 mg/ml A549 cell extract was supplemented with energy cocktail and incubated for one hour at room temperature on 30ul PAV-951, PAV-0805 Resins in triplicate, or a control resin consisting of an affi-gel matrix bound to itself. The resins were then washed 100x with buffer to remove nonspecifically bound material and then eluted overnight at room temperature with 100ul 100uM PAV-951 or PAV-0805 supplemented with energy cocktail. The eluates were run on SDS PAGE

and analyzed by silver stain, western blot, and MSMS. **Figure 3A** shows the silver stain protein pattern in the eluate. **Figure 3 B** shows a Venn Diagram of gene products identified by MSMS in the PAV-951 and PAV-0805 resin eluates, grouped by the proteins only identified in the PAV-951 target, proteins identified in both the PAV-951 and PAV-0805 targets, and proteins only identified in the PAV-0805 target. Proteins identified in the negative control resin eluates were removed from the analysis. Proteins detected in any of the triplicate samples were included in the analysis. **Figure 3 C** shows western blots for ALDH1A1, GSTP1, PDI, PSMB5 MDH, and YWHAZ in eluate samples. **Figure 3D** shows quantitation of the protein bands detected by western blot, where triplicates have been averaged and error bars denote standard deviation.

The identified proteins, minus those identified in the control resin eluate, were then searched in a cancer hallmarks database[30]. The hallmarks database identifies gene sets which are associated with the ten classic hallmarks of cancer— replicative immortality, reprogramming energy metabolism, resisting cell death, tumor promoting inflammation, tissue invasion and metastasis, sustained angiogenesis, evading immune destruction, evading growth suppressors, genome instability, and sustaining proliferating signaling[30–32]. Significant enrichment was found for the hallmarks of reprogramming energy metabolism ($p< 0.00001$) and resisting cell death ($p<0.01$) in the PAV-0805 target (see **Figure 4**, left hand side modified from Menyhart et. al.)

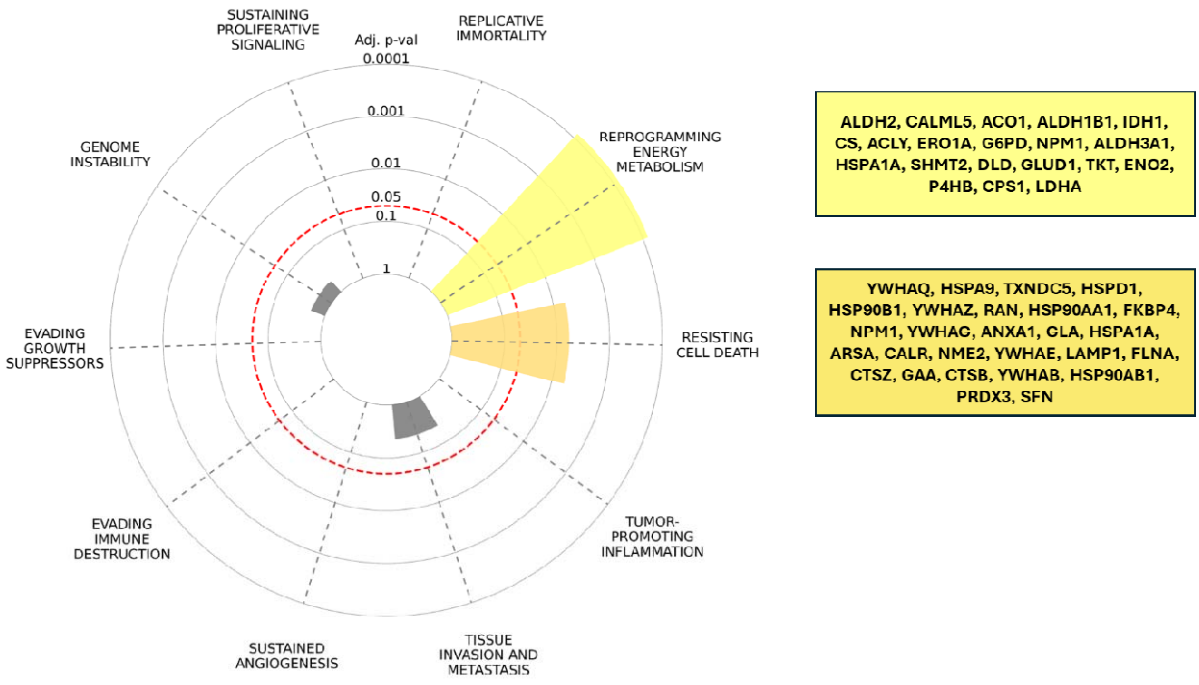

Figure 5. Association of PAV-0805 target complex with the Hallmarks of Cancer. Proteins identified by MSMS as comprising the target of PAV-0805 were searched in a database for sets of genes associated with the hallmarks of cancer[30]. Association with a particular cancer hallmark is based on the enrichment of hallmark-associated genes identified relative to a reference set. Significant enrichment was found for the cancer hallmarks of reprogramming energy metabolism and resisting cell death. The boxes on the right indicate the proteins identified by MSMS in the PAV-0805 resin eluate which are associated with these hallmarks.

A549 (non-small cell lung cancer), HT29 (colon cancer), and U251 (brain cancer) cells were treated with DMSO or 1uM PAV-805 for 20 hours, then lysate was prepared for DRAC. By silver stain, PAV-0805 resin eluate appeared to target a similar complex from the three cell types examined (See **Figure 6A**). Western blot identified KAP1, PDI, and YWHAZ in the resin eluates from all three starting materials (See **Figures 6B and 6C**). ALDH1A1 was detected in the eluate derived from A549 and HT29 cells, and but not eluate derived from U251 cells (See **Figures 6B and 6C**). The target appeared enriched with PAV-0805 treatment with more protein detected in conditions where cells had been treated with the

assembly modulator compound than DMSO (See **Figures 6A-C**). This phenomenon was particularly pronounced for a 100 kDa band detected by western blot for KAP1 (See **Figures 6B** and **6C**).

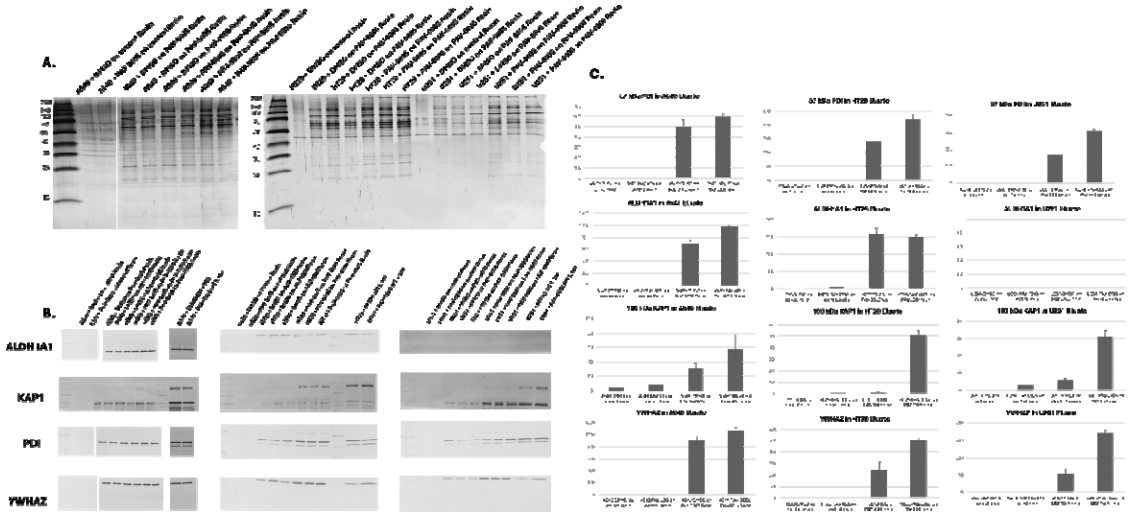

Figure 6. Comparison of A549, HT29, and U251 Treated with Vehicle or PAV-0805 by DRAC. A549, HT29, and U251 cells were treated with DMSO or 1uM PAV-0805, and cell lysate was prepared. 30ul of 5 mg/ml cell extract was supplemented with energy cocktail and incubated for one hour at room temperature on 30ul PAV-0805 Resin in triplicate, or a control resin consisting of an affi-gel matrix bound to itself. The resins were then washed 100x with buffer to remove nonspecifically bound material and then eluted overnight at room temperature with 100ul PAV-0805 supplemented with energy cocktail. The eluates were run on SDS PAGE and analyzed by silver stain and western blot. **Figure 3A** shows the silver stain protein pattern in the eluates. **Figure 3B** shows western blots for ALDH1A1, KAP1, PDI, and YWHAZ in eluate samples. **Figure 3C** shows quantitation of the protein bands detected by western blot, where triplicates have been averaged and error bars denote standard deviation.

A photocrosslinker analog of PAV-0805, modified to contain a diazirine and a biotin group at the same position where resin had been attached, was synthesized to provide insight on which protein component was directly bound and which components were indirectly bound as part of a multi-protein complex held together through non-covalent interactions. PAV-0805-treated A549, HT29, and U251 cell

extracts were used as starting material for this experiment due to the enhancement of target detected by DRAC under the treated conditions. Cell extract was incubated with the PAV-0805 photocrosslinker in triplicate, or with a negative control crosslinker compound which contained the biotin and diazirine, but no assembly modulator compound. The extract was then exposed to UV light for 10 minutes, creating a covalent bond between the diazirine moiety of the modified compound and the protein to which was directly bound. The crosslinked samples were then divided into two aliquots. One aliquot was left native, while the other aliquot was denatured with SDS and heat, and then the aliquots were both diluted with column buffer containing excess Triton-X-100, a non-denaturing detergent which forms micelles with the free SDS. Streptavidin beads were used to precipitate the biotinylated material, with the denatured samples revealing the direct drug-binding protein(s) and the native samples revealing all proteins contained in the drug binding multi-protein complex. Western blot identified PDI in both the native and denatured samples and KAP1 in the native but not denatured samples (see **Figure 7**).

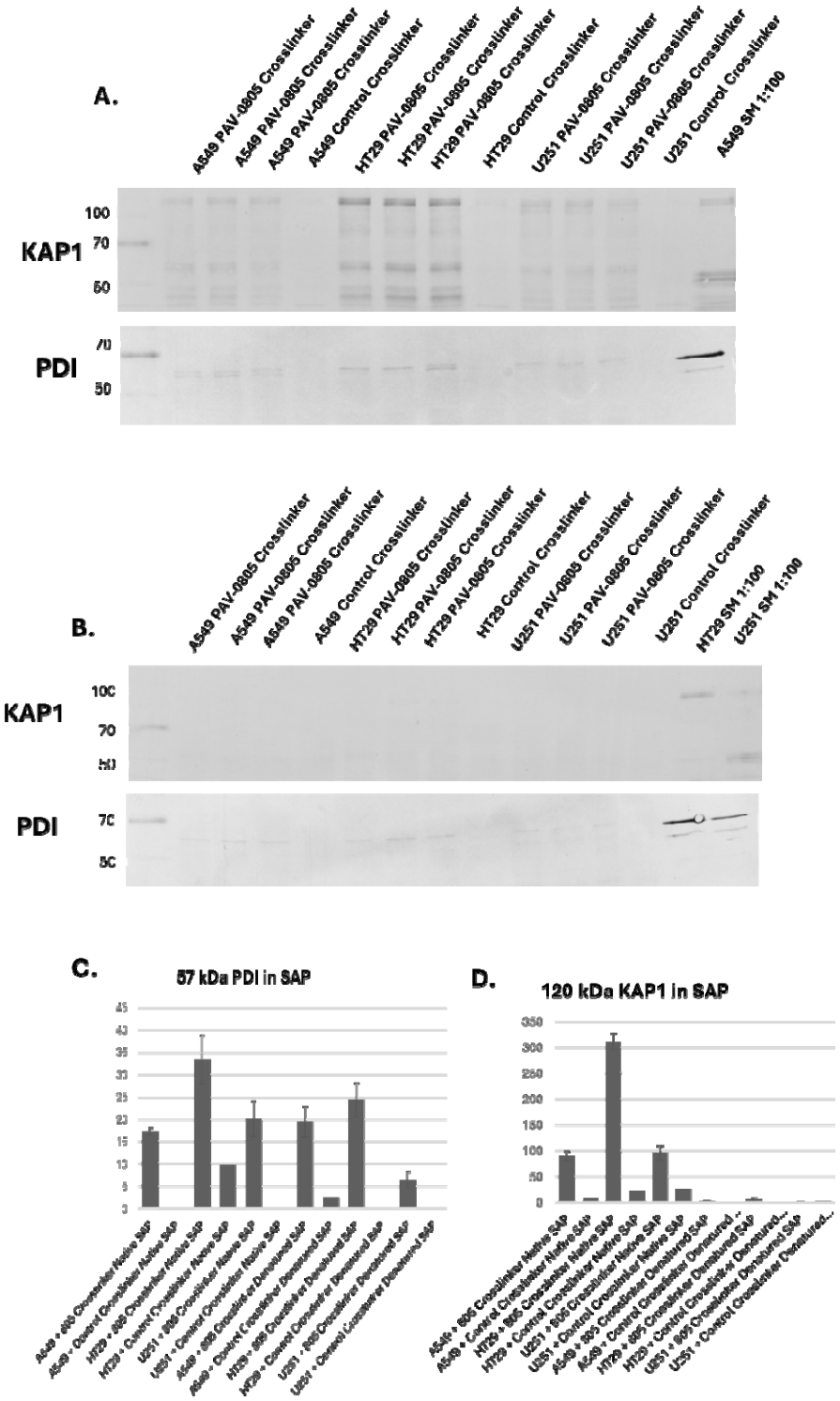

Figure 7. Identification of PDI as a direct target and KAP1 as an indirect target of PAV-0805. Cell extract was prepared from A549, HT29, and U251 cells that were treated with PAV-

0805 for 20 hours. The cell extract was incubated with a photocrosslinker analog of PAV-0805 then exposed to UV light. The crosslinked samples were divided into two aliquots, one kept one native and one treated with denatured conditions, and precipitated with streptavidin beads. **Figure 7A** shows the western blots for KAP1 and PDI in native streptavidin precipitation (SAP) samples. **Figure 7B** shows the western blots for KAP1 and PDI in denatured SAP samples. **Figure 7C** shows quantitation of the 57 kDa protein band detected by western blot for PDI in the SAP where triplicates have been averaged and standard error is denoted by error bars. **Figure 7D** shows quantitation of the 120kDa protein band detected by western blot for KAP1 in the SAP where triplicates have been averaged and standard error is denoted by error bars.

Discussion

SAR Exploration Leads to PAV-0805

Our data shows that PAV-0805 is broadly cytotoxic against the NCI-60 cancer cell lines without toxicity to PBMCs. Furthermore, a nontoxic dose of PAV-0805 significantly inhibited tumor growth and reduced metastasis in the 4T1 allograft mouse model for triple negative metastatic breast cancer. The anti-cancer effects were significant even when treatment began late and the tumor was already in its exponential growth phase. The anti-cancer activity of PAV-0805 was comparable to Paclitaxel, which is a first-line treatment for metastatic breast cancer in humans[33].

The primary challenge for advancing oncology drugs is how to develop a compound that kills cancer cells and spares normal cells. The uniqueness of assembly modulating compounds is the ability to selectively target particular biochemical features of aberrant assembly machines that are strongly associated with disease states and not those present in normal assembly machines carrying out homeostatic functions in healthy cells. In other words, a cell which is following its programming for homeostasis would not be affected when exposed to a compound that selectively targets aberrant protein

assembly. However, a cancerous cell whose survival requires protein machinery that has departed from maintenance of homeostasis would experience growth inhibition and/or cytotoxicity when exposed to this compound.

PAV-951, the original assembly modulator with pan-cancer activity, showed broad but modest activity against the NCI-60 tumor cell panel and in the xenograft mouse models for A549 lung cancer and HT29 colon cancer[1]. SAR exploration demonstrated that small changes to the chemical structure of PAV-951 could eliminate or expand upon the anti-cancer activity, as observed for a structurally unrelated assembly modulator effective in cellular and animal models of ALS[25,26]. Multiple analogs were identified with no anti-cancer activity whatsoever, indicating specificity for the active structures. Multiple analogs were identified which were 100% lethal for every single tumor line examined. The SAR showing improved safety among analogs with comparably potent anti-tumor cytotoxicity which indicates that toxicity to healthy cells is not an inherent feature of the assembly modulator anti-cancer mechanism.

The enhanced safety observed for PAV-0805 with maintenance of efficacy, is consistent with our general model for drugs targeting assembly machines, and with our specific model for oncogenesis as a transition from normal to aberrant assembly machines. Our findings underscore that the functional impact of a protein is reflected in the “company that it keeps”, i.e., the assembly machine, which is not easily discernable from the specific characteristics of the gene sequences or protein product itself. This concept is consistent with the observation that some proteins exhibit “moonlighting” functions that may not have been identified by their sequence alone[34–37]. Whether due to covalent post-translational modifications, intrinsically unfolded domains, or alternate pathways of protein biogenesis, there is growing recognition that gene expression needs to be parsed in a more granular fashion to understand the complex biology arising from protein heterogeneity, particularly within multi-protein complexes[37–41]. While viruses achieve this goal through natural selection in struggle with their hosts, our phenotypic screen started from where the viruses left off: allowing us to drive drug discovery to cancer specifically.

Connecting Protein Assembly Modulation to the Hallmarks of Cancer

The MS-MS results revealing enrichment in specific cancer hallmark-associated gene products for PAV-0805 provides context regarding which cancer-associated biochemical pathways are impacted by assembly modulation. The enrichment analysis showed that the proteins found to be targeted by PAV-0805were associated with the cancer hallmarks of resisting programmed cell death and reprogramming energy metabolism[1,30–32]. Targeting of these cancer hallmarks may explain the observed novel pan-cancer activity of the compounds starting with the PAV-951 parent and more advanced analogs culminating to date in PAV-0805. The unique target and mechanism may be a path to developing a treatment which targets cancer cells more broadly and yet more specifically without killing healthy cells.

Resisting programmed cell death is a fundamental hallmark of cancer[31,32]. Restoring a crucial control point that allow inappropriately proliferating cells to be driven to programmed cell death provides a novel, broad, and potent anti-cancer mechanism. Future studies will focus on precisely how that reversal is achieved and how it interfaces with pathways that are currently far better understood.

Gene products implicated in reprogramming energy metabolism represent a second cancer hallmark significantly enriched in the PAV-0805 drug resin eluate. It is likely not a co-incidence that metabolic reprogramming is implicated in viral infection as well[16,42–44]. Reprogramming energy metabolism is critical for creating a cellular microenvironment that serves the need of both viruses and cancer, allowing each to bypass homeostasis[16,31,42]. Activity against abnormal energy metabolism pathways may also explain the potent activity of our compounds in metastasis models (both in cell culture and in the late-treatment allograft group) as cellular reprogramming is a critical component of the epithelial-to-mesenchymal transition which drives the development of metastasis[45,46]. Finally it should be noted that the target multi-protein complex of PAV-0805, as well as other assembly modulator compounds, is both transient and energy-dependent[1,5,25]. Further work will be needed to explore these associations.

Characterizing the PAV-0805 Target

Like its parent compound PAV-951, PAV-0805 targets a dynamic multi-protein complex. When the DRAC eluates containing the target complexes of PAV-951 and PAV-905 were compared, they were found to contain overlapping, but distinct sets of proteins. Some proteins, such as PSMB5, MDH, and GSTP1 which were identified in the PAV-951 target, were not found in the PAV-0805 target. Other proteins, such as PDI, were found in both targets, but significantly less bound and eluted from PAV-0805. Other proteins, such as YWHAZ were found in greater amounts in the PAV-0805 eluate.

The differences in protein composition detected in the PAV-0805 target may indicate increased selectivity of the compound for particular subsets of proteins that are found in particular multi-protein complexes. Increased selectivity towards a particular target complex may correspond to decreased toxicity, as the potential for “collateral damage” of off-target effects decreases in tandem. Further studies will reveal whether the functional changes in PAV-805 target are due to higher affinity to the aberrant cancer-specific multi-protein complex target or due to loss of a separate shared target found in a subset of healthy cells.

ALDH was detected, by western blot, in the eluate from A549 cell lysate and not in the eluate from U251 cancer cell lysate. This indicates that the target may have a different composition from one cancer cell to another. This is consistent with an upstream, allosteric mechanism of action where compound treatment restores an aberrant assembly machine to its normal function/composition regardless of which proteins have gone awry as part of the cancer’s cellular reprogramming. The differences and similarities in the target from one cancer cell to another, including in how those cells respond to compound treatment, could reveal much about PAV-0805 and the mechanism of assembly modulators more broadly.

When DMSO versus PAV-0805 treated cell extracts were compared on the PAV-0805 resin, a 100kDa KAP1 band was detected by western blot in the PAV-0805 target. We thought the enrichment of this particular form of KAP1 in the target with PAV-0805 treatment was notable given the described roles of KAP1 in the literature. KAP1 is an allosteric modulator involved in a variety of protein-protein interactions an array of functions including transcriptional activation of HIV, T-cell development, DNA damage repair, as a transcriptional co-repressor for many genes, and as a ligase for post translational modifications such as ubiquitination and SUMOlyation[47,48]. Studies have shown increased levels of KAP1 in many types of cancer and high levels of KAP1 correlate with a lower survival rate[49–51]. However, other described functions of KAP1 are tumor suppressive and promote autophagy[48,52,53]. KAP1 is described in the literature as directly binding with cancer-implicated proteins including MDM2, TRIM24, FBP1, MAGE-A3, MAGE-C2, HSP70, and TWIST1[53–57]. The diversity of functions that KAP1 displays appears to be, at least in part, through its assembly into different multi-protein complexes that carry out different objectives. That treatment with PAV-0805 triggers that recruitment of a *particular* 100 kDa form of KAP1 into the PAV-0805 target, may be a critical step in the compound's mechanism. These dynamics may not only be specific for particular forms of KAP1, but also may vary from one cancer to another.

Photocrosslinking revealed that, within the PAV-0805 multi-protein complex target, KAP1 is not the direct drug binding protein, which is a subset of PDI. PDI proteins are multi-functional and they carry out distinct catalytic activities that include facilitating the isomerization of disulfide bonds, the oxidation of thiols, and oxidative protein folding[58]. PDI is described in the literature as undergoing a number of post-translational modifications[58–60]. Some of these modifications are linked to particular diseases including, for example, that S-nitrosylation of PDI is associated with neurodegeneration and S-glutathionylation of PDI is associated with cancer [59–61].

If viruses evolved to parse out the relationship between post-translational heterogeneity (including formation of multi-protein complexes and post-translational modifications) and disease, then the target of PAV-0805 likely sits at the parallel intersection of post-translational heterogeneity and

homeostasis. The interactions that associate PAV-0805 to PDI and PDI to the other proteins in the target, could reveal a multitude of information on the molecular basis for homeostasis. These insights would be inaccessible through other, more conventional, approaches.

Future studies

Further work is needed to optimize this pan-cancer assembly modulator series as a potential human cancer therapeutic. PAV-0805 is an advanced analog in terms of achieving a balance of efficacy and safety, but it is not the most potent anti-cancer compound we have identified in the series. Further SAR exploration may be needed identify a compound which maximizes efficacy while retaining or further enhancing safety. We have not yet begun to undertake the exhaustive process of off-target liability profiling and GLP toxicology, which are required prior to a human clinical study. Nevertheless, we are encouraged that the results we have seen thus far hold the potential to yield a non-toxic cure for cancer, through a novel mechanism.

Methods

National Cancer Institute 60 Cell Line Screen

In the NCI-60 screen, up to 60 cancer cell lines (CCRF-CEM, HL-60(TB), K-562, MOLT-4, RPMI-8226, SR, A549/ATCC, EKVX, HOP-62, HOP-92, NCI-H226, NCI-H23, NCI-H322M, NCI-H460, NCI-H522, COLO 205, HCC-2998, HCT-116, HCT-15, HT29, KM12, SW-620, SF-268, SF-295, SF-539, SNB-19, SNB-75, U251, LOX IMVI, MALME-3M, M14, MDA-MB-435, SK-MEL-2, SK-MEL-28, SK-MEL-5, UACC-257, UACC-62, IGROV1, OVCAR-3, OVCAR-4, OVCAR-5, OVCAR-8, NCI/ADR-RES, SK-OV-3, 786-0, A498, ACHN, CAKI-1, RXF 393, SN12C, TK-10, UO-31, PC-3, DU-145, MCF7, MDA-MB-231/ATCC, HS 578T, BT-549, T-47D, MDA-MB-468) are grown.

Two methods have been used to assess anti-tumor cytotoxicity in the NCI-60 screen.

In the Classic Screen (method used through September 2023), cells were grown for 24 hours then treated with vehicle or compound, or fixed in situ with TCA, to represent a measurement of the cell population for each cell line at the time of drug addition. The treated cells were grown for an additional 48 hours before being fixed in situ with TCA. Fixed cells were then stained with Sulforhodamine B. Absorbance was read to determine cell viability of compound-treated cells relative to both the time at which treatment began and to untreated cells at the end of the study. The NCI-60 screen was initially conducted at a single dose of 2.5uM, but was subsequently repeated with a dose titration.

The human tumor cell lines of the cancer screening panel are grown in RPMI 1640 medium containing 5% fetal bovine serum and 2 mM L-glutamine. For a typical screening experiment, cells are inoculated into 96 well microtiter plates in 100 μL at plating densities ranging from 5,000 to 40,000 cells/well depending on the doubling time of individual cell lines. After cell inoculation, the microtiter plates are incubated at 37° C, 5 % CO2, 95 % air and 100 % relative humidity for 24 h prior to addition of experimental drugs.

After 24 h, two plates of each cell line are fixed in situ with TCA, to represent a measurement of the cell population for each cell line at the time of drug addition (Tz). Experimental drugs are solubilized in dimethyl sulfoxide at 400-fold the desired final maximum test concentration and stored frozen prior to use. At the time of drug addition, an aliquot of frozen concentrate is thawed and diluted to twice the desired final maximum test concentration with complete medium containing 50 μg/ml gentamicin

Following drug addition, the plates are incubated for an additional 48 h at 37°C, 5 % CO2, 95 % air, and 100 % relative humidity. For adherent cells, the assay is terminated by the addition of cold TCA. Cells are fixed in situ by the gentle addition of 50 μl of cold 50 % (w/v) TCA (final concentration, 10 % TCA) and incubated for 60 minutes at 4°C. The supernatant is discarded, and the plates are washed five times with tap water and air dried. Sulforhodamine B (SRB) solution (100 μl) at 0.4 % (w/v) in 1 % acetic acid is added to each well, and plates are incubated for 10 minutes at room temperature. After staining, unbound dye is removed by washing five times with 1 % acetic acid and the plates are air dried. Bound stain is

subsequently solubilized with 10 mM trizma base, and the absorbance is read on an automated plate reader at a wavelength of 515 nm. For suspension cells, the methodology is the same except that the assay is terminated by fixing settled cells at the bottom of the wells by gently adding 50 μl of 80 % TCA (final concentration, 16 % TCA).

In the HTS384 Screen (method used after September 2023), the sixty human tumor cell lines of the cancer screening panel are grown in RPMI 1640 medium containing 5% fetal bovine serum and 2 mM L-glutamine. To initiate a screen, 40 μl of cells are inoculated into the wells of white 384-well microtiter plates at plating densities ranging from 250 to 2,500 cells/well, depending on the doubling time of individual cell lines. After inoculation, the microtiter plates are incubated at 37°C with 5% CO^2 and 95% relative humidity for 24 h before the addition of controls and test agents. Prior to a screen, the test agents and controls are solubilized in dimethyl sulfoxide (DMSO) at 400-fold the final test concentration and stored frozen in polypropylene 384-well microtiter plates.

Twenty-four hours after cell line inoculation, acoustic dispensing is used to transfer 100 nl of DMSO (0.25% (v/v), final) into the wells of microtiter plates, each containing a single cell line. Subsequently, 40 μl of CellTiter-Glo are dispensed into the wells, according to the manufacturer's protocol. Luminescence is measured to assess cell viability at the time of drug addition (time zero, Tz). Acoustic dispensing is also used to transfer 100 nl of controls and test agents (400-fold dilution, final) into duplicate microtiter plates for each cell line to achieve technical replicates. Controls in each microtiter plate include vehicle, 100% cytotoxicity (1 μM Staurosporin NSC755774 and 3 μM Gemcitabine NSC613327 [n = 8]), and five concentrations of doxorubicin (NSC123127, 25 μM [n = 2], 2.5 μM [n = 1], 250 nM [n = 2], 25 nM [n = 1], 2.5 nM [n = 2]. Following the delivery of controls and test agents, the microtiter plates are incubated for 72 h at 37°C with 5 % CO^2 and 95% relative humidity. After 72 h of exposure, 40 μl of CellTiter-Glo are dispensed into the wells of the microtiter plates and luminescence is measured, according to the manufacturer's protocol, to assess cell viability.

For both methods, using the seven absorbance measurements [time zero, (Tz), control growth, (C), and test growth in the presence of drug at the five concentration levels (Ti)], the percentage growth is calculated at each of the drug concentrations levels. Percentage growth is calculated as:

[(Ti-Tz)/(C-Tz)] x 100 for concentrations for which Ti>/=Tz

[(Ti-Tz)/Tz] x 100 for concentrations for which Ti<Tz.

Three dose response parameters are calculated for each experimental agent. Growth inhibition of 50 % (GI50) is calculated from [(Ti-Tz)/(C-Tz)] x 100 = 50, which is the drug concentration resulting in a 50% reduction in the net protein increase (as measured by SRB staining) in control cells during the drug incubation. The drug concentration resulting in total growth inhibition (TGI) is calculated from Ti = Tz. The LC50 (concentration of drug resulting in a 50% reduction in the measured protein at the end of the drug treatment as compared to that at the beginning) indicating a net loss of cells following treatment is calculated from [(Ti-Tz)/Tz] x 100 = -50. Values are calculated for each of these three parameters if the level of activity is reached; however, if the effect is not reached or is exceeded, the value for that parameter is expressed as greater or less than the maximum or minimum concentration tested.

PAV-951, PAV-0383, PAV-0384 were assessed in the Classic Screen. All others were assessed by the HTS384 screen.

Cytotoxicity Assessment on PBMCs and H9 Lymphoma

Healthy human PBMCs and H9 cells were seeded at a density of 5,000 cells/well and treated with either DMSO or compound, at concentrations of 2.5uM, 5uM, 10uM, and 20uM. The cells were incubated at 37oC for 72 hours then cell viability was measured using an AlamarBlue™ assay.

Mouse Safety

For the intraperitoneal MTD study, female Balb/c mice aged 8-10 weeks were randomly divided into treatment groups with three animals per group. Animals in each treatment group were weighed and received one IP injection of 0.1-0.15mL containing either vehicle (10% DMSO, 45% propylene glycol, 45% sterile water), or varying doses compound. Animals were observed from day 0 until day 3 for clinical signs of toxicity. Animals were euthanized after 72 hours and were examined externally and internally by a pathologist for abnormalities in organ weight and tissue damage. Blood samples were sent for a complete blood count bioanalysis. MTD was determined to be the dose at which no signs of toxicity were observed by any parameters.

Mouse Allograft

A suspension of 0.1×10^6 cells were implanted into the mammary fat pad of normal balb/c mice. Size of the tumor was measured using a digital Vernier caliper. Tumor volume was calculated as the [Length (L) × Width (W) ^{2}] /2, where length (L) is the largest diameter of the tumor and width (W) is the smallest diameter. Animals were treated by IP injection daily with either vehicle (N=6), 2 mg/kg Paclitaxel (N=6), or 10mg/kg PAV-0805 (N=6), beginning when the tumor volume reached 50mm^3. An additional late treatment group (N=3) received vehicle until the tumor volume reached 500mm^3, and were subsequently treated with 10mg/kg PAV-0805 daily. Tumor growth inhibition was calculated based on the following formula:

$$\% \text{ TGI} = \frac{\{(TV_{vehicle}\ \text{Final} - TV_{vehicle}\ \text{Initial}) - (TV_{treatment}\ \text{Final} - TV_{treatment}\ \text{Initial})\}}{(TV_{vehicle}\ \text{Final} - TV_{vehicle}\ \text{Initial})} \times 100$$

Animals were sacrificed once the tumor in the vehicle-treated group reached a volume of 2000mm^3. Lung tissues were isolated and visually observed for metastatic cancer cell colonies.

Drug Resin Affinity Chromatography

A549, HT29, or U251 cells were grown in minimum essential media (UCSF) with 10% FBS and 1% Penstrep for 48 hours. In some conditions cells were treated with PAV-0805 for 20 hours. Cells were scraped into cold phosphate buffered saline (PBS) (10mM sodium phosphate, 150 mM sodium chloride pH 7.4), then spun at 1,000 rpm for 10 minutes until pelleted. The PBS was decanted and the pellet resuspended in a low salt buffer (10mM HEPES pH 7.6, 10mM NaCl, 1mM MgAc with 0.35% Tritonx100) then centrifuged at 10,000 rpm for 10 minutes at 4o C. The post-mitochondrial supernatant was removed and adjusted to a concentration of approximately 5 mg/ml unless otherwise stated and equilibrated in a physiologic column buffer (50 mM Hepes ph 7.6, 100 mM KAc, 6 mM MgAc, 1 mM EDTA, 4mM TGA). The extract was supplemented with an energy cocktail (to a final concentration of 1mM rATP, 1mM rGTP, 1mM rCTP, 1mM rUTP, creatine phosphate and 5 ug/mL creatine kinase). 30 ul of extract was then incubated for one hour at 22oC on 30 ul of affi-gel resin coupled to PAV-951, PAV-0805, or a 4% agarose matrix (control). The input material was collected and the resin was then washed with 3 ml column bufffer. The resins were eluted overnight at 22oC in 100ul column buffer containing 100uM PAV-951 or PAV-0805 with the energy cocktail. Eluate samples were sent for MSMS analysis.

Chemical Photocrosslinking

Cell extract was prepared as above then adjusted to a protein concentration of approximately 2 mg/ml in column buffer (50 mM Hepes pH 7.6, 100 mM KAc, 6 mM MgAc, 1 mM EDTA, 4mM TGA). 70ul of 2uM stock of photocrosslinker analogs of PAV-905 or PAV-906 chemically modified to contain biotin and a diazirine group or a control containing the biotin and diazarine but not assembly modulator compound prepared in column buffer were added to 70ul of extract, incubated for one hour at on ice, then exposed to ultraviolet light for 10 minutes on ice. After crosslinking, samples were divided in two 60 ul aliquots and

one set was denatured by adding 6ul of 10% SDS, 0.75 ul DTT, and boiling for 10 minutes. Both native and denatured aliquots were then diluted in 1200 ul column buffer containing 0.1% triton. 5 ul of magnetic streptavidin beads were added to all samples and mixed for one hour at room temperature to capture all biotinylated proteins and co-associated proteins. Samples were placed on a magnetic rack to hold the beads in placed and washed three times with 1mL of column buffer containing 0.1% triton. After washing, beads were resuspended in 40 ul of gel loading buffer containing SDS and analyzed by western blot for PDI and KAP1.

Silver Stain

SDS/PAGE gels were incubated overnight in a fixative (50% methanol, 10% acetic acid, 40% water), then for an hour in 50% methanol (done as two washes), and an hour in water (done as two washes). The gels were sensitized in 0.02% sodium thiosulfate for one minute then washed twice for 30 seconds with water. The gels were incubated for 30 minutes in cold 0.1% silver nitrate with 0.02% formaldehyde then washed twice for 30 seconds. The gels were developed in 3% sodium carbonate with 0.02% formaldehyde. The developed gels showing the pattern of protein bands was scanned and the image was analyzed.

Western blotting

SDS/PAGE gels were transferred in Towbin buffer (25mM Tris, 192mM glycine, 20% w/v methanol) to polyvinylidene fluoride membrane, blocked in 1% bovine serum albumin (BSA) in PBS, incubated overnight at 4 degrees Celsius in a 1:1,000 dilution of 100ug/mL affinity-purified primary IGG to PDI, HIV Gag, KAP1, MDH, YWHAZ in 1% BSA in PBS containing 0.1% Tween-20 (PBST). Membranes were then washed twice in PBST and incubated for two hours at room temperature in a 1:5000 dilution of secondary anti-rabbit or anti-mouse antibody coupled to alkaline phosphatase in PBST. Membranes were washed two more times in PBST then incubated in a developer solution prepared from 100 uL of 7.5 mg/mL 5-bromo-4-chloro-3-indolyl phosphate dissolved in 60% dimethyl formamide (DMF) in water and

100ul of 15 mg/ml nitro blue tetrazolium dissolved in 70% DMF in water, adjusted to 50mL with 0.1 Tris (pH 9.5) and 0.1 mM magnesium chloride. Membranes were scanned and the integrated density of protein band was measured on ImageJ. Averages and the standard deviation between repeated experiments were calculated and plotted on Microsoft Excel.

MSMS Analysis

Samples were processed by SDS PAGE using a 10% Bis-ttris NuPAGE gel with the MES buffer system. The mobility region was excised and washed with 25 mM ammonium bicarbonate followed by 15mM acetonitrile. Samples were reduced with 10 mM dithoithreitol and 60 degrees Celsius followed by alkylation with 5o mM iodacetamide at room temperature. Samples were then digested with trypsin (Promega) overnight (18 hours) at 37 oC then quenched with formic acid and desalted using an Empore SD plate. Half of each digested sample was analyzed by LC-MS/MS with a Waters NanoAcquity HPLC system interfaced to a ThermoFisher Q Exactive. Peptides were loaded on a trapping column and eluted over a 75uM analytical column at 350 nL/min packed with Luna C18 resin (Phenomenex). The mass spectrometer was operated in a data dependent mode, with the Oribtrap operating at 60,000 FWHM and 15,000 FWHM for MS and MS/MS respectively. The fifteen most abundant ions were selected for MS/MS.

Data was searched using a local copy of Mascot (Matrix Science) with the following parameters: Enzyme: Trypzin/P; Database: SwissProt Human (concatenated forward and reverse plus common contaminants); Fixed modification: Carbamidomethyl (C) Variable modifications: Oxidation (M), Acetyl (N-term), Pyro-Glu (N-term Q), Deamidation (N/Q) Mass values: Monoisotopic; Peptide Mass Tolerance: 10 ppm; Fragment Mass Tolerance: 0.02 Da; Max Missed Cleavages: 2. The data was analyzed by label free quantitation (LFQ) and spectral count methods. LFQ intensity values of each condition were measured in triplicate and compared against each other to generate log2 fold change values for each

combination of conditions. Spectral counts were filtered for a 1% protein/peptide false discovery rate requiring 2 unique peptides per protein.

The data set was further adjusted by subtraction of spectral counts for specific proteins observed in the control resin, and subtraction of proteins that were not found in all triplicate-repeat samples. The adjusted dataset was searched for enrichment of cancer hallmarks in the cancerhallmarks.com dataset as described in https://doi.org/10.1016/j.jpha.2024.101065.

Supplemental Figures

Protein	Gene	MW	Control	PAV-0805	PAV-0805	PAV-0805
Desmoplakin	DSP	332 kDa	73	98	49	16
Endoplasmic reticulum chaperone BiP	HSPA5	72 kDa	4	61	32	54
Aldehyde dehydrogenase, dimeric NADP-preferring	ALDH3A1	50 kDa	0	29	16	29
Hornerin	HRNR	282 kDa	39	42	16	10
Protein disulfide-isomerase A3	PDIA3	57 kDa	0	22	17	26
Junction plakoglobin	JUP	82 kDa	29	26	21	12
Thioredoxin reductase 1, cytoplasmic	TXNRD1	71 kDa	0	19	14	22
Heat shock cognate 71 kDa protein	HSPA8	71 kDa	3	19	15	20
14-3-3 protein zeta/delta	YWHAZ	28 kDa	0	20	13	21
Adenosylhomocysteinase	AHCY	48 kDa	0	17	13	22
Heat shock 70 kDa protein 1A	HSPA1A	70 kDa	0	16	13	23
Actin, cytoplasmic 2	ACTG1	42 kDa	13	19	12	20
14-3-3 protein theta	YWHAQ	28 kDa	0	19	9	17
Aldehyde dehydrogenase, mitochondrial	ALDH2	56 kDa	0	18	11	13
Aldehyde dehydrogenase 1A1	ALDH1A1	55 kDa	0	14	7	19
Creatine kinase M-type	CKM	43 kDa	7	16	10	14
Glucose-6-phosphate 1-dehydrogenase	G6PD	59 kDa	0	13	5	19
Serine hydroxymethyltransferase, mitochondrial	SHMT2	56 kDa	0	11	8	15
Filamin-B	FLNB	278 kDa	0	12	8	10
Desmoglein-1	DSG1	114 kDa	15	16	8	5
14-3-3 protein beta/alpha	YWHAB	28 kDa	0	0	11	18
Calreticulin OS=Homo sapiens	CALR	48 kDa	0	11	7	10

Elongation factor 2	EEF2	95 kDa	3	11	10	7
Lactotransferrin	LTF	78 kDa	15	16	8	4
14-3-3 protein gamma	YWHAG	28 kDa	0	12	0	16
ATP-citrate synthase	ACLY	121 kDa	0	12	7	8
Myosin-9	MYH9	227 kDa	0	22	0	4
Alpha-enolase	ENO1	47 kDa	6	11	5	9
Lysozyme C	LYZ	17 kDa	8	10	6	9
Annexin A2	ANXA2	39 kDa	9	11	8	5
Heat shock protein HSP 90-alpha	HSP90AA1	85 kDa	0	7	9	8
Myosin-10	MYH10	229 kDa	0	23	0	0
Peroxiredoxin-1	PPRDX1	22 kDa	0	10	7	6
Small ribosomal subunit protein RACK1	RACK1	35 kDa	0	8	6	9
Serpin B3	SERPINB3	45 kDa	11	14	4	5
Gamma-enolase	ENO2	47 kDa	0	9	3	10
Filaggrin-2	FLG2	248 kDa	14	12	7	3
Lysosomal alpha-glucosidase	GAA	105 kDa	0	11	5	6
Serotransferrin	TF	77 kDa	11	12	5	5
Cystatin-A	CSTA	11 kDa	10	10	6	5
Haptoglobin	HP	45 kDa	6	7	6	8
Immunoglobulin heavy constant gamma 3	IGHG3	49 kDa	7	10	6	5
Protein disulfide-isomerase	P4HB	57 kDa	0	11	0	9
Protein-glutamine gamma-glutamyltransferase E	TGM3	77 kDa	9	9	5	5
60 kDa heat shock protein, mitochondrial	HSPD1	61 kDa	0	7	2	9
Plakophilin-1	PKP1	83 kDa	11	10	8	0
Elongation factor 1-alpha 1	EEF1A1	50 kDa	0	6	5	6
Hemoglobin subunit alpha	HBA1 PE=1 SV=2	15 kDa	8	7	3	6
Immunoglobulin heavy constant gamma 2	IGHG2	44 kDa	6	10	0	6
Nucleolin OS=Homo sapiens	NCL	77 kDa	0	4	0	12
Peroxiredoxin-2	PRDX2	22 kDa	3	7	6	3
Putative phospholipase B-like 2	PLBD2	65 kDa	0	5	4	6
Protein-glutamine gamma-glutamyltransferase K	TGM1	90 kDa	7	10	5	0
UDP-glucose 6-dehydrogenase	UGDH	55 kDa	0	6	0	9
Arginase-1	ARG1	35 kDa	3	5	5	4
Heat shock protein HSP 90-beta	HSP90AB1	83 kDa	0	8	0	6
Zinc-alpha-2-glycoprotein	AZGP1	34 kDa	15	8	0	5
Cathepsin D	CTSD	45 kDa	4	5	4	4

Glyceraldehyde-3-phosphate dehydrogenase	GAPDH	36 kDa	5	9	0	4
Immunoglobulin heavy constant alpha 1	IGHA1	43 kDa	5	3	5	5
Pyruvate kinase PKM	PKM	58 kDa	4	7	0	6
Cornifin-B	SPRR1B	10 kDa	5	8	3	2
A-kinase anchor protein 12	AKAP12	191 kDa	0	6	3	3
Annexin A1	ANXA1	39 kDa	0	5	7	0
Glutamate dehydrogenase 1, mitochondrial	GLUD1	61 kDa	0	3	3	6
Lipocalin-1	LCN1	19 kDa	6	5	3	4
Lupus La protein	SSB	47 kDa	0	0	4	8
Apolipoprotein D	APOD	21 kDa	5	7	0	4
Caspase-14	CASP14	28 kDa	8	7	0	4
Citrate synthase, mitochondrial	CS	52 kDa	0	4	3	4
Dihydrolipoyl dehydrogenase, mitochondrial	DLD	54 kDa	0	4	0	7
Eukaryotic translation initiation factor 5A-1	EIF5A	17 kDa	0	3	3	5
14-3-3 protein sigma	SFN	28 kDa	0	0	0	11
Fatty acid-binding protein 5	FABP5	15 kDa	5	5	3	2
Filaggrin	FLG	435 kDa	12	10	0	0
Protein S100-A8	S100A8	11 kDa	7	3	3	4
Protein S100-A9	S100A9	13 kDa	6	5	3	2
Apolipoprotein A-I	APOA1	31 kDa	0	4	3	2
Histone H2B type 1-K	H2BC12	14 kDa	3	4	0	5
Leukocyte elastase inhibitor	SERPINB1	43 kDa	0	2	4	3
Elongation factor Tu, mitochondrial	TUFM	50 kDa	0	2	2	5
T-complex protein 1 subunit zeta	CCT6A	58 kDa	0	3	2	3
Desmocollin-1	DSC1	100 kDa	10	8	0	0
Gasdermin-A	GSDMA	49 kDa	0	5	3	0
Proliferating cell nuclear antigen	PCNA	29 kDa	0	3	0	5
Polymeric immunoglobulin receptor	PIGR	83 kDa	8	8	0	0
Serpin B12	SERPINB12	46 kDa	3	8	0	0
Triosephosphate isomerase	TPI1	27 kDa	4	4	0	4
Thioredoxin domain-containing protein 5	TXNDC5	48 kDa	0	3	0	5
Polyubiquitin-B	UBB	26 kDa	7	0	0	8
Catalase	CAT	60 kDa	4	7	0	0
Drebrin	DBN1	71 kDa	0	7	0	0
Filamin-A	FLNA	281 kDa	0	7	0	0
High mobility group protein B1	HMGB1	25 kDa	0	3	0	4
Heat shock 70 kDa protein 4	HSPA4	94 kDa	0	3	0	4

Adenosylhomocysteinase 3	AHCYL2	67 kDa	0	6	0	0
Arylsulfatase A	ARSA	54 kDa	0	3	0	3
Cathepsin B	CTSB	38 kDa	0	3	3	0
Glutathione synthetase	GSS	52 kDa	0	6	0	0
Immunoglobulin lambda constant 2	IGLC2	11 kDa	3	3	0	3
NAD(P)H-hydrate epimerase	NAXE	32 kDa	0	2	0	4
Small ribosomal subunit protein eS7	RPS7	22 kDa	0	4	0	2
Protein S100-A4	S100A4	12 kDa	0	2	0	4
Alpha-1-antitrypsin	SERPINA1	47 kDa	0	6	0	0
Transketolase	TKT	68 kDa	0	6	0	0
14-3-3 protein epsilon	YWHAE	29 kDa	0	0	0	6
ATP synthase F(1) complex subunit alpha, mitochondrial	ATP5F1A	60 kDa	0	2	0	3
ATP synthase F(1) complex subunit beta, mitochondrial	ATP5F1B	57 kDa	0	0	5	0
T-complex protein 1 subunit epsilon	CCT5	60 kDa	0	3	0	2
T-complex protein 1 subunit theta	CCT8	60 kDa	0	0	0	5
Procathepsin L	CTSL	38 kDa	0	0	0	5
Rab GDP dissociation inhibitor beta	GDI2	51 kDa	0	0	2	3
Histone H3.1	H3C1	15 kDa	0	3	0	2
Hepatoma-derived growth factor	HDGF	27 kDa	0	0	0	5
Peroxisomal multifunctional enzyme type 2	HSD17B4	80 kDa	0	3	0	2
Endoplasmin	HSP90B1	92 kDa	0	5	0	0
Insulin-degrading enzyme	IDE	118 kDa	0	5	0	0
GTP-binding nuclear protein Ran	RAN	24 kDa	0	0	0	5
Protein S100-A6	S100A6	10 kDa	0	2	0	3
Small proline-rich protein 2D	SPRR2D	8 kDa	0	3	2	0
Small proline-rich protein 3	SPRR3	18 kDa	0	2	3	0
Complement C3	C3	187 kDa	3	4	0	0
T-complex protein 1 subunit beta	CCT2	57 kDa	0	0	0	4
Carbamoyl-phosphate synthase [ammonia], mitochondrial	CPS1	165 kDa	0	4	0	0
Dermcidin	DCD	11 kDa	2	2	2	0
Alpha-galactosidase A	GLA	49 kDa	0	4	0	0
Lysine--tRNA ligase	KARS1	68 kDa	0	0	0	4
Prolactin-inducible protein	PIP	17 kDa	0	2	0	2
Peptidyl-prolyl cis-trans isomerase B	PPIB	24 kDa	0	0	2	2
Lysosomal Pro-X carboxypeptidase	PRCP	56 kDa	0	4	0	0
Thioredoxin-dependent peroxide reductase, mitochondrial	PRDX3	28 kDa	0	0	0	4

Hsc70-interacting protein	ST13	41 kDa	0	2	0	2
Tubulin-folding cofactor B	TBCB	27 kDa	0	0	0	4
Cytoplasmic aconitate hydratase	ACO1	98 kDa	0	0	0	3
Neuroblast differentiation-associated protein AHNAK	AHNAK	629 kDa	0	3	0	0
Arachidonate 12-lipoxygenase, 12R-type	ALOX12B	80 kDa	2	3	0	0
Alpha-amylase 1B	AMY1B	58 kDa	4	3	0	0
Bleomycin hydrolase	BLMH	53 kDa	0	3	0	0
Corneodesmosin	CDSN	52 kDa	0	3	0	0
Cathepsin Z	CTSZ	34 kDa	0	3	0	0
Neutrophil defensin 1	DEFA1	10 kDa	3	3	0	0
Histone H2A type 1-B/E	H2AC4	14 kDa	0	0	0	3
Histone H4	H4C1	11 kDa	4	0	0	3
Heterogeneous nuclear ribonucleoprotein U	HNRNPU	91 kDa	0	0	0	3
Stress-70 protein, mitochondrial	HSPA9	74 kDa	0	0	3	0
10 kDa heat shock protein, mitochondrial	HSPE1	11 kDa	0	0	0	3
Kallikrein-7	KLK7	28 kDa	2	3	0	0
Protein KPLCE	KPLCE	26 kDa	6	3	0	0
L-lactate dehydrogenase A chain	LDHA	37 kDa	0	3	0	0
Galectin-1	LGALS1	15 kDa	0	0	0	3
Loricrin	LORICRIN	26 kDa	3	3	0	0
Unconventional myosin-Id	MYO1D	116 kDa	0	3	0	0
Nucleoside diphosphate kinase B	NME2	17 kDa	0	0	0	3
Protein POF1B	POF1B	68 kDa	0	3	0	0
Protein S100-A7	S100A7	11 kDa	6	0	0	3
Single-stranded DNA-binding protein, mitochondrial	SSBP1	17 kDa	0	3	0	0
Aldo-keto reductase family 1 member C3	AKR1C3	37 kDa	0	0	0	2
Aldehyde dehydrogenase X, mitochondrial	ALDH1B1	57 kDa	0	0	0	2
Calmodulin-like protein 5	CALML5	16 kDa	0	2	0	0
T-complex protein 1 subunit delta	CCT4	58 kDa	0	0	0	2
Ceruloplasmin	CP	122 kDa	0	2	0	0
Scavenger receptor cysteine-rich domain-containing protein DMBT1	DMBT1	261 kDa	0	2	0	0
ERO1-like protein alpha	ERO1A	54 kDa	0	0	0	2
Peptidyl-prolyl cis-trans isomerase FKBP4	FKBP4	52 kDa	0	0	0	2
Ferritin heavy chain	FTH1	21 kDa	0	2	0	0

Neutral alpha-glucosidase AB	GANAB	107 kDa	0	0	0	2
Gamma-glutamyl hydrolase	GGH	36 kDa	0	0	0	2
3-hydroxyacyl-CoA dehydrogenase type-2	HSD17B10	27 kDa	0	0	0	2
Isocitrate dehydrogenase [NADP] cytoplasmic	IDH1	47 kDa	0	0	0	2
Lysosome-associated membrane glycoprotein 1	LAMP1	45 kDa	0	2	0	0
Nucleophosmin OS=Homo sapiens	NPM1	33 kDa	0	0	0	2
Small ribosomal subunit protein uS2B	RPSA2	33 kDa	0	2	0	0
Superoxide dismutase [Cu-Zn]	SOD1	16 kDa	3	0	0	2
Fibrinogen beta chain	FGB	56 kDa	3	0	0	0
Fibrinogen gamma chain	FGG	52 kDa	2	0	0	0
Hemoglobin subunit beta	HBB	16 kDa	6	0	0	0
Inter-alpha-trypsin inhibitor heavy chain H1	ITIH1	101 kDa	3	0	0	0
Phosphatidylethanolamine-binding protein 1	PEBP1	21 kDa	2	0	0	0
Suprabasin	SBSN	61 kDa	4	0	0	0
Serpin A12	SERPINA12	47 kDa	3	0	0	0
Thioredoxin	TXN	12 kDa	2	0	0	0

Supplemental Figure 1. MSMS analysis of PAV-0805 Resin Eluate. PAV-0805 was coupled to a resin and DRAC was performed using A549 cell lysate. The eluates from a control resin eluted with PAV-0805 and triplicate-repeat eluates from the PAV-0805 resin eluted with PAV-0805 were sent for MSMS analysis. Identified proteins and spectral counts are provided in the table. 181 proteins were identified overall. 115 proteins were not detected in the control. 29 proteins were not detected in the control and were identified in all three triplicate samples. The table lists the proteins and spectral counts detected by MSMS, ordered by average spectral count, and where red to green conditional formatting has been applied to indicate the relative number of spectra detected.

References

1. Lingappa, A. F. *et al.* Small molecule protein assembly modulators with pan-cancer therapeutic efficacy. *Open Biol.* **14**, 240210 (2024).
2. Heckmann, C. M. & Paradisi, F. Looking Back: A Short History of the Discovery of Enzymes and How They Became Powerful Chemical Tools. *ChemCatChem* **12**, 6082–6102 (2020).
3. Nirenberg, M. Historical review: Deciphering the genetic code – a personal account. *Trends Biochem. Sci.* **29**, 46–54 (2004).
4. Blobel, G. Protein targeting (Nobel lecture). *Chembiochem Eur. J. Chem. Biol.* **1**, 86–102 (2000).
5. Michon, M. *et al.* A pan-respiratory antiviral chemotype targeting a transient host multi-protein complex. *Open Biol.* **14**, 230363 (2024).
6. Lingappa, U. F. *et al.* Host–rabies virus protein–protein interactions as druggable antiviral targets. *Proc. Natl. Acad. Sci.* **110**, (2013).
7. Reed, J. C. *et al.* Identification of an Antiretroviral Small Molecule That Appears To Be a Host-Targeting Inhibitor of HIV-1 Assembly. *J. Virol.* **95**, e00883-20 (2021).
8. Lingappa, J. R., Hill, R. L., Wong, M. L. & Hegde, R. S. A Multistep, ATP-dependent Pathway for Assembly of Human Immunodeficiency Virus Capsids in a Cell-free System. *J. Cell Biol.* **136**, 567–581 (1997).
9. Du, L. *et al.* A viral assembly inhibitor blocks SARS-CoV-2 replication in airway epithelial cells. *Commun. Biol.* **7**, 486 (2024).
10. Priyamvada, L. *et al.* New methylene blue derivatives suggest novel anti-orthopoxviral strategies. *Antiviral Res.* **191**, 105086 (2021).
11. Reed, J. C. *et al.* HIV-1 Gag co-opts a cellular complex containing DDX6, a helicase that facilitates capsid assembly. *J. Cell Biol.* **198**, 439–456 (2012).
12. Lingappa, V. R. & Lingappa, J. R. Recent insights into biological regulation from cell-free protein-synthesizing systems. *Mt. Sinai J. Med. N. Y.* **72**, 141–160 (2005).

13. Javier, R. T. & Butel, J. S. The History of Tumor Virology. *Cancer Res.* **68**, 7693–7706 (2008).

14. Morales-Sánchez, A. & Fuentes-Pananá, E. Human Viruses and Cancer. *Viruses* **6**, 4047–4079 (2014).

15. Krump, N. A. & You, J. Molecular mechanisms of viral oncogenesis in humans. *Nat. Rev. Microbiol.* **16**, 684–698 (2018).

16. Purdy, J. G. & Luftig, M. A. Reprogramming of cellular metabolic pathways by human oncogenic viruses. *Curr. Opin. Virol.* **39**, 60–69 (2019).

17. Münger, K. *et al.* Mechanisms of Human Papillomavirus-Induced Oncogenesis. *J. Virol.* **78**, 11451–11460 (2004).

18. McLaughlin-Drubin, M. E. & Münger, K. The human papillomavirus E7 oncoprotein. *Virology* **384**, 335–344 (2009).

19. Boyer, S. N., Wazer, D. E. & Band, V. E7 protein of human papilloma virus-16 induces degradation of retinoblastoma protein through the ubiquitin-proteasome pathway. *Cancer Res.* **56**, 4620–4624 (1996).

20. White, E. A. *et al.* Systematic identification of interactions between host cell proteins and E7 oncoproteins from diverse human papillomaviruses. *Proc. Natl. Acad. Sci.* **109**, (2012).

21. Flores, E. R., Allen-Hoffmann, B. L., Lee, D. & Lambert, P. F. The human papillomavirus type 16 E7 oncogene is required for the productive stage of the viral life cycle. *J. Virol.* **74**, 6622–6631 (2000).

22. Riley, R. R. *et al.* Dissection of human papillomavirus E6 and E7 function in transgenic mouse models of cervical carcinogenesis. *Cancer Res.* **63**, 4862–4871 (2003).

23. Mir, B. A. *et al.* Increased expression of HPV-E7 oncoprotein correlates with a reduced level of pRb proteins via high viral load in cervical cancer. *Sci. Rep.* **13**, 15075 (2023).

24. Müller-Schiffmann, A., Trossbach, S. V., Lingappa, V. R. & Korth, C. Viruses as ‘Truffle Hounds’: Molecular Tools for Untangling Brain Cellular Pathology. *Trends Neurosci.* **44**, 352–365 (2021).

25. Yu, S. F. *et al.* Protein Assembly Modulation: A New Approach to Amyotrophic Lateral Sclerosis (ALS) Therapeutics. *J. Exp. Neurol.* **5**, 210–230 (2024).

26. Yu, S. F. *et al.* An ALS assembly modulator signature in peripheral blood mononuclear cells: implications for ALS pathophysiology, therapeutics, and diagnostics. *Clin. Proteomics* **22**, (2025).

27. Yang, Y. *et al.* Immunocompetent mouse allograft models for development of therapies to target breast cancer metastasis. *Oncotarget* **8**, 30621–30643 (2017).

28. Yang, S., Zhang, J. J. & Huang, X.-Y. Mouse models for tumor metastasis. *Methods Mol. Biol. Clifton NJ* **928**, 221–228 (2012).

29. Chavez, K. J., Garimella, S. V. & Lipkowitz, S. Triple negative breast cancer cell lines: One tool in the search for better treatment of triple negative breast cancer. *Breast Dis.* **32**, 35–48 (2011).

30. Menyhart, O., Kothalawala, W. J. & Győrffy, B. A gene set enrichment analysis for the cancer hallmarks. *J. Pharm. Anal.* 101065 (2024) doi:10.1016/j.jpha.2024.101065.

31. Hanahan, D. & Weinberg, R. A. The Hallmarks of Cancer. *Cell* **100**, 57–70 (2000).

32. Hanahan, D. & Weinberg, R. A. Hallmarks of Cancer: The Next Generation. *Cell* **144**, 646–674 (2011).

33. Bishop, J. F. *et al.* Paclitaxel as first-line treatment for metastatic breast cancer. The Taxol Investigational Trials Group, Australia and New Zealand. *Oncol. Williston Park N* **11**, 19–23 (1997).

34. Jeffery, C. J. Multitalented actors inside and outside the cell: recent discoveries add to the number of moonlighting proteins. *Biochem. Soc. Trans.* **47**, 1941–1948 (2019).

35. Jeffery, C. J. Protein moonlighting: what is it, and why is it important? *Philos. Trans. R. Soc. B Biol. Sci.* **373**, 20160523 (2018).

36. Jeffery, C. J. Enzymes, pseudoenzymes, and moonlighting proteins: diversity of function in protein superfamilies. *FEBS J.* **287**, 4141–4149 (2020).

37. Jeffery, C. J. Protein species and moonlighting proteins: Very small changes in a protein's covalent structure can change its biochemical function. *J. Proteomics* **134**, 19–24 (2016).

38. Hegde, R. Regulation of protein biogenesis at the endoplasmic reticulum membrane. *Trends Cell Biol.* **9**, 132–137 (1999).

39. Hegde, R. S. & Lingappa, V. R. Membrane Protein Biogenesis: Regulated Complexity at the Endoplasmic Reticulum. *Cell* **91**, 575–582 (1997).

40. Alpert, E. *et al.* Multifunctionality of Prostatic Acid Phosphatase in Prostate Cancer Pathogenesis. *Biosci. Rep.* BSR20211646 (2021) doi:10.1042/BCJ20200944.

41. Uversky, V. N. Dancing Protein Clouds: The Strange Biology and Chaotic Physics of Intrinsically Disordered Proteins. *J. Biol. Chem.* **291**, 6681–6688 (2016).

42. Allen, C. N. S., Arjona, S. P., Santerre, M. & Sawaya, B. E. Hallmarks of Metabolic Reprogramming and Their Role in Viral Pathogenesis. *Viruses* **14**, 602 (2022).

43. Thyrsted, J. & Holm, C. K. Virus-induced metabolic reprogramming and innate sensing hereof by the infected host. *Curr. Opin. Biotechnol.* **68**, 44–50 (2021).

44. Liu, X., Zhu, C., Wang, Y., Wei, F. & Cai, Q. KSHV Reprogramming of Host Energy Metabolism for Pathogenesis. *Front. Cell. Infect. Microbiol.* **11**, 621156 (2021).

45. Faubert, B., Solmonson, A. & DeBerardinis, R. J. Metabolic reprogramming and cancer progression. *Science* **368**, eaaw5473 (2020).

46. Morandi, A., Taddei, M. L., Chiarugi, P. & Giannoni, E. Targeting the Metabolic Reprogramming That Controls Epithelial-to-Mesenchymal Transition in Aggressive Tumors. *Front. Oncol.* **7**, (2017).

47. Iyengar, S. & Farnham, P. J. KAP1 Protein: An Enigmatic Master Regulator of the Genome. *J. Biol. Chem.* **286**, 26267–26276 (2011).

48. Randolph, K., Hyder, U. & D'Orso, I. KAP1/TRIM28: Transcriptional Activator and/or Repressor of Viral and Cellular Programs? *Front. Cell. Infect. Microbiol.* **12**, 834636 (2022).

49. Addison, J. B. *et al.* KAP1 Promotes Proliferation and Metastatic Progression of Breast Cancer Cells. *Cancer Res.* **75**, 344–355 (2015).

50. Cui, Y. *et al.* High Levels of KAP1 Expression Are Associated with Aggressive Clinical Features in Ovarian Cancer. *Int. J. Mol. Sci.* **16**, 363–377 (2014).

51. Yu, C. *et al.* KAP-1 is overexpressed and correlates with increased metastatic ability and tumorigenicity in pancreatic cancer. *Med. Oncol.* **31**, 25 (2014).

52. Neo, S. H. *et al.* TRIM28 Is an E3 Ligase for ARF-Mediated NPM1/B23 SUMOylation That Represses Centrosome Amplification. *Mol. Cell. Biol.* **35**, 2851–2863 (2015).

53. Yang, Y. *et al.* Acetylated hsp70 and KAP1-mediated Vps34 SUMOylation is required for autophagosome creation in autophagy. *Proc. Natl. Acad. Sci.* **110**, 6841–6846 (2013).

54. Fong, K., Zhao, J. C., Song, B., Zheng, B. & Yu, J. TRIM28 protects TRIM24 from SPOP-mediated degradation and promotes prostate cancer progression. *Nat. Commun.* **9**, 5007 (2018).

55. Jin, X. *et al.* MAGE-TRIM28 complex promotes the Warburg effect and hepatocellular carcinoma progression by targeting FBP1 for degradation. *Oncogenesis* **6**, e312–e312 (2017).

56. Wang, C. *et al.* MDM2 interaction with nuclear corepressor KAP1 contributes to p53 inactivation. *EMBO J.* **24**, 3279–3290 (2005).

57. Wei, C. *et al.* Tripartite motif containing 28 (TRIM28) promotes breast cancer metastasis by stabilizing TWIST1 protein. *Sci. Rep.* **6**, 29822 (2016).

58. Ali Khan, H. & Mutus, B. Protein disulfide isomerase a multifunctional protein with multiple physiological roles. *Front. Chem.* **2**, (2014).

59. Townsend, D. M. *et al.* Nitrosative Stress–Induced *S* -Glutathionylation of Protein Disulfide Isomerase Leads to Activation of the Unfolded Protein Response. *Cancer Res.* **69**, 7626–7634 (2009).

60. Uehara, T. *et al.* S-Nitrosylated protein-disulphide isomerase links protein misfolding to neurodegeneration. *Nature* **441**, 513–517 (2006).

61. Rahman, N. S. A. *et al.* Functions and mechanisms of protein disulfide isomerase family in cancer emergence. *Cell Biosci.* **12**, 129 (2022).

Acknowledgements

We thank the National Cancer Institute for running the NCI-60 screening data shown.

Funding

Support for these studies was provided by Prosetta Biosciences, Inc.